

RAL 86018
Copy 1 R61
RAL-86-018
ACCN: 147847

Science and Engineering Research Council
Rutherford Appleton Laboratory
CHILTON, DIDCOT, OXON, OX11 0QX

RAL-86-018

Measurement of the Velocity of Sound in Crystals by Pulsed Neutron Diffraction.

B.T.M. Willis, C.J. Carlile, R.C. Ward, W.I.F. David and M.W. Johnson

LIBRARY
Rutherford Appleton Laboratory
14 APR 1986
LA

March 1986

© Science and Engineering
Research Council 1986

The Science and Engineering Research Council does not accept any responsibility for loss or damage arising from the use of information contained in any of its reports or in any communication about its tests or investigations.

Measurement of the Velocity of Sound
in Crystals by Pulsed Neutron Diffraction

by

B T M Willis

Chemical Crystallography Laboratory
University of Oxford
Oxford, England

and

C J Carlile, R C Ward,
W I F David and M W Johnson

Rutherford Appleton Laboratory
Chilton, Oxfordshire
England

Submitted to Physical Review Letters

Abstract

The diffraction method of observing elementary excitations in crystals has been applied to the study of one-phonon thermal diffuse scattering from pyrolytic graphite on a high resolution pulsed neutron diffractometer . The variation of the phase velocity of sound as a function of direction in the crystal has been determined for the out-of-plane modes. This is a quick and efficient method of determining sound velocities in crystals under extreme conditions.

In the diffraction method of studying elementary excitations in single crystals by neutron inelastic scattering, the energy dispersion relations of the crystal can be derived from the measured momentum distribution of the scattered neutrons alone, without the need for energy analysis. The method was first suggested by Elliott and Lowde in 1955 and applied to the study of both magnons [see Samuelson (1968)] and phonons [see Hohlwein (1977)].

Because of experimental limitations the diffraction method was never fully developed. However, the High Resolution Powder Diffractometer HRPD [Johnson and David (1985)] installed on the pulsed spallation neutron source ISIS at the Rutherford Appleton Laboratory represents an advance in instrumentation which enables the method to be exploited further. The principal advantage of HRPD is that the detector, in back-scattering geometry, simultaneously covers a wide range of scattering angles. Combined with the broad wavelength band incident upon the sample and the pulsed nature of the beam, one-phonon inelastic scattering can be investigated without moving the crystal.

In this letter we present measurements of the acoustic phonons in pyrolytic graphite using the diffraction method to reveal hitherto unseen structure in the scattering, and we derive the sound velocity for the out-of-plane modes and its variation with direction.

Although HRPD is designed primarily to study crystalline powders by time of flight neutron diffraction, the sample in the present case was a single crystal of pyrolytic graphite. High resolution is achieved by locating the sample 96 metres from the neutron source and then detecting the diffracted neutrons as a function of their time of flight at scattering angles 2θ close to 180° . The detector is a one-dimensional array comprising 20 annular rings covering a range of scattering angles from 170° to 178° in increments of 0.4° . The crystal, in the form of a plate of thickness 2 mm and face area 40 mm x 30 mm, had a mosaic spread of 0.4° .

Figure 1 illustrates the experimental set up. The [001] axis of the crystal lies in the horizontal scattering plane. The element of the detector which is located precisely at $2\theta = 2\theta_B$, where θ_B is the Bragg angle, records the Bragg reflections shown in Figure 2a. The other elements of the detector measure the thermal diffuse scattering at progressively larger displacements $\Delta\theta$ from the Bragg condition, an example of which is shown in Figure 2b. For each detector element at a given offset angle $\Delta\theta$ the thermal diffuse scattering intensity rises to a maximum on each side of the Bragg position: one peak corresponds to neutron energy gain ($\epsilon = -1$) and the other to neutron energy loss ($\epsilon = +1$). [The central peaks in Figure 2(b) are caused by cross-talk from the detector element recording the intense Bragg reflection]. The relationship between $\Delta\theta$ and Δt , where Δt is the displacement in time of flight of the thermal diffuse scattering peak from the Bragg peak, can be used to determine the sound velocity from the theory outlined below. A multiple plot of data from all detector elements is shown in Figure 3 in the time regime corresponding to the (004) reflection. The increasing separation of the thermal diffuse scattering peaks on both sides of the Bragg position as $\Delta\theta$ increases can be clearly seen.

We can interpret the results on graphite by extending the standard theory of one-phonon inelastic scattering of thermal neutrons (Lovesey 1985). Full details of these calculations will be published elsewhere (Willis 1986).

Let \underline{k}_0 , \underline{k} be the wave vectors of the incident and scattered neutrons respectively. If 2θ is the scattering angle (i.e. the angle between \underline{k}_0 and \underline{k}) and $2\theta_B$ is the Bragg angle, then the wave vector diagram in reciprocal space is as illustrated in Figure 4. Here P is the reciprocal-lattice point and PQ [PQ'] is a phonon of wave vector \underline{q} [\underline{q}'] involved in the scattering process for which the neutron loses energy ($\epsilon = +1$). At shorter values of the wave vector \underline{k}_0 it is also possible for scattering to occur with energy gain ($\epsilon = -1$). In the figure we show schematically the scattering surfaces, or loci of the end-points of \underline{q} , for these two processes. The momentum conservation condition requires that

$$\underline{\tau} + \underline{q} = \underline{k} - \underline{k}_0, \quad (1)$$

where $\underline{\tau}$ is the reciprocal lattice vector. The energy conservation condition implies, for $k \approx k_0$ and for small values of q , that

$$k - k_0 = -\epsilon\beta(\zeta)q \quad (2)$$

where $\beta(\zeta)$ is the ratio of the phase velocity $c_s(\zeta)$ in the crystal to the neutron velocity v_n (Willis, Carlile and Ward, 1986). c_s is a function of the direction of propagation ζ , but for simplicity we have drawn the scattering surfaces in Figure 4 for the case in which c_s is independent of ζ .

In HRPD the incident flight path is 50 times greater than the scattered flight path, so that the total flight time of neutrons from source to detector is almost independent of the magnitude of the scattered wave vector \underline{k} . We assume, therefore, that all inelastic scattering events sharing the same incident wave vector \underline{k}_0 are recorded in the same time channel. Thus lines in reciprocal space which are parallel to \underline{k} correspond to loci of constant time of flight. Scattering occurring along such a line is integrated by the detector into the same time channel.

From Figure 4 we see that there is a range of incident wave vectors \underline{k}_0 (and a corresponding range of times of flight) for which one-phonon scattering is forbidden. The boundary between the forbidden and allowed regions of scattering occurs when the points Q and Q' coalesce and \underline{q} and \underline{q}' are therefore coincident. In this special case a single phonon only contributes to the scattering and its angle to the [001] direction is given by ζ where

$$\zeta = \theta_B - \arctan \left[\frac{\Delta\theta \operatorname{cosec}^2 \theta_B}{\Delta t / t_B} - \cot \theta_B \right] \quad (3)$$

In equation (3) the width of the forbidden region has been expressed in terms of the separation in time Δt of the edge of the forbidden region from the Bragg position at $t=t_B$. The relation between Δt and $\Delta\theta$ (Willis 1986) is

$$\frac{\Delta t}{t_B} = \frac{\Delta\theta \operatorname{cosec}^2 \theta_B}{-\epsilon \left| \frac{\Delta\theta}{\Delta\theta} \right| (\beta^2 - 1)^{-\frac{1}{2}} + \cot \theta_B} \quad (3)$$

In Figure 5 we plot the experimental values of $\Delta t/t_B$ versus $\Delta\theta$ for the 00ℓ reflections ($\ell = 4, 6, 8, 10$) of graphite. Only the data for the two quadrants having $\epsilon(\Delta\theta/|\Delta\theta|) \leq 0$ have been plotted. Applying equations (3) and (4) to the data allows us to derive the phase velocity as a function of direction, as indicated in Figure 6. The phase velocity of the out-of-plane modes (Bowman and Krumhansl, 1958), with polarization normal to the close-packed layers, rises steeply as \underline{q} approaches the [001] direction. The sound velocities along [001] as determined by neutron inelastic scattering and from ultrasound measurements are also indicated (Nicklow, Wakabayashi and Smith, 1972).

In our experiment the scattering vector \underline{Q} ($= \underline{k} - \underline{k}_0$) was always within 10° of the [001] direction. The scattering from the in-plane modes is suppressed by the $|\underline{Q} \cdot \underline{e}_j(\underline{q})|^2$ term in the scattering cross-section (Lovesey, 1985) since the polarisation vector $\underline{e}_j(\underline{q})$ of these modes was nearly normal to \underline{Q} .

We have demonstrated that the one-phonon thermal diffuse scattering in single crystals rises to sharp, well-defined maxima in reciprocal space. This effect is observed with neutrons and not with X-rays, and is associated with the restrictions imposed on the one-phonon scattering by the momentum and energy conservation laws for neutrons. By measuring the separation of these maxima as a function of scattering angle and for different reciprocal lattice points using a time-of-flight diffractometer, we have deduced the velocity of the out-of-plane modes of vibration and the variation of this velocity with direction of propagation in pyrolytic graphite. When fully commissioned the HRPD diffractometer will be furnished with a detector with complete azimuthal symmetry about the incident neutron beam. By aligning the crystal so that the Bragg angle is precisely 90° the Bragg reflection will be directed back along the incident beam path. The one-phonon scattering will then be completely symmetrical on each side of the detector and the effects of cross-talk will be removed. More importantly observations can be made along a number of symmetry directions simultaneously without the need to reorient the crystal. This is a general method of determining sound velocities in crystals, and promises to be of particular value for measurements under extreme environmental conditions such as temperature or pressure.

We are pleased to acknowledge discussions with B A Dasannacharya, A J Leadbetter, D K Ross, P Schofield and E Steichele. A Freund kindly loaned the pyrolytic graphite crystal. The work of one of the authors (BTMW) was supported by a research contract from AERE, Harwell, England.

Bowman J C and Krumhansl J A (1958). J Phys Chem Solids 6, 367.

Elliott R J and Lowde R D (1955) Proc Roy Soc A230, 46.

Hohlwein D (1978). Proceedings of a Symposium on Neutron Inelastic Scattering IAEA Vienna, October 1977; 197.

Johnson M W and David W I F. Rutherford Appleton Laboratory Report 1985 RAL-85-112.

Lovesey S W (1985) "Theory of Neutron Scattering from Condensed Matter" Volume 1 Clarendon Press: Oxford.

Nicklow R, Wakabayashi N and Smith H G (1972) Phys Rev B5, 4951.

Samuelson E J (1968). Physics Letters 26A 160.

Willis B T M, Carlile C J and Ward R C (1986). Acta Cryst A. To be published.

Willis B T M (1986). Acta Cryst A to be published.

Figure Captions

- Figure 1: The experimental set-up. The [001] axis of the pyrolytic graphite crystal is at 3° to the incoming neutron beam. The waveband choppers prevent frame overlap between successive pulses.
- Figure 2: (a) Bragg peaks from the (00 l) planes of pyrolytic graphite recorded in the detector element lying at the Bragg scattering angle $2\theta_B = 174^\circ$. (b) One-phonon thermal diffuse scattering peaks recorded in a detector element offset from the Bragg scattering angle by $\Delta 2\theta = 2\theta - 2\theta_B = 3.2^\circ$.
- Figure 3: The scattering pattern around the (004) reflection from pyrolytic graphite showing the variation in the thermal diffuse scattering intensity as a function of time-of-flight and scattering angle offset $\Delta 2\theta$ from the Bragg angle.
- Figure 4: A representation of the scattering process in reciprocal space showing the hyperbolic scattering surfaces and, as a shaded area, the forbidden region in which no thermal diffuse scattering is observed. For clarity the scattering angle 2θ is drawn as $\sim 80^\circ$ rather than $\sim 174^\circ$, as in the backscattering geometry used. The point S is the termination of the scattered vector \underline{k} for the elastic scattering process ($k=k_0$).
- Figure 5: The displacements in time $\Delta t/t_B$ of the one-phonon thermal diffuse scattering peaks in graphite around the 00 l reciprocal lattice points plotted as a function of the offset $\Delta\theta$ from the Bragg angle.
- Figure 6: The phase velocity $c(\zeta)$ of the out-of-plane modes in pyrolytic graphite as a function of the angle between [001] and the propagation direction. The line is a least squares straight line fit to the data [\bullet]. The symbol O indicates the velocity derived from phonon dispersion curve measurements by neutron scattering and \circ the velocity determined by ultrasound measurements (Nicklow et al 1972).

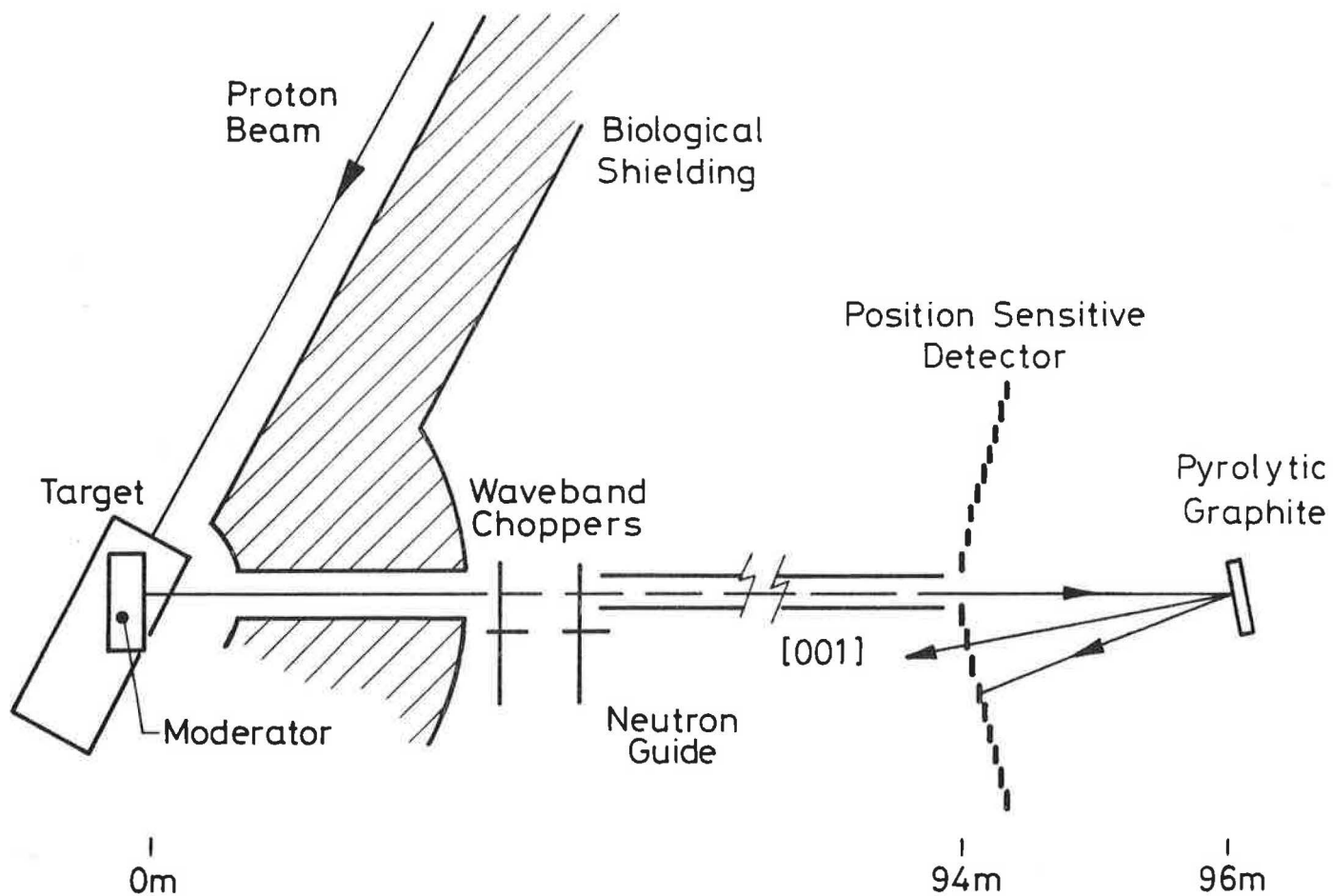


Figure 1: The experimental set-up. The [001] axis of the pyrolytic graphite crystal is at 3° to the neutron beam. The waveband choppers prevent frame overlap between successive pulses.

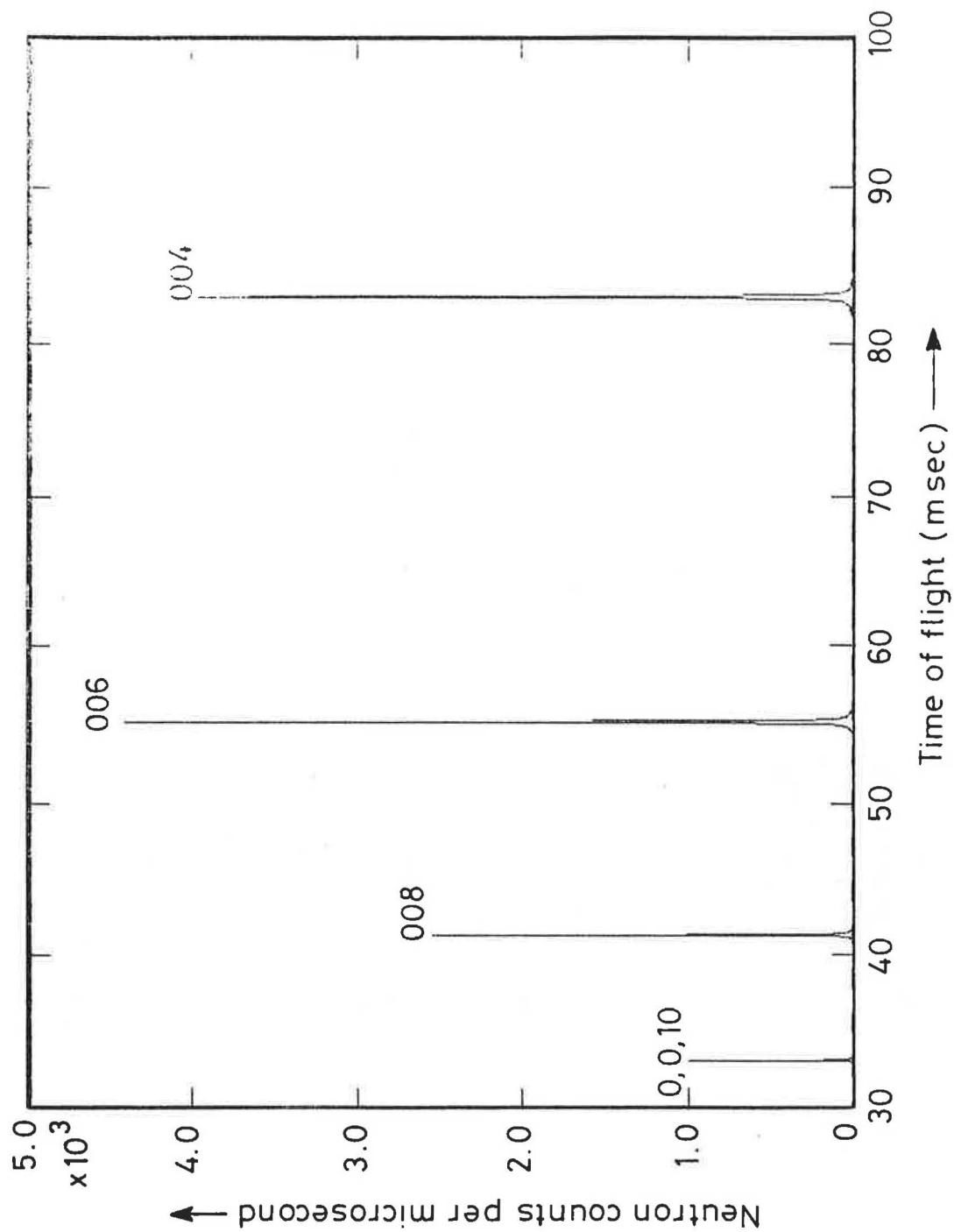


Figure 2: (a) Bragg peaks from the (00 l) planes of pyrolytic graphite recorded in the detector element lying at the Bragg scattering angle $2\theta_B = 174^\circ$.

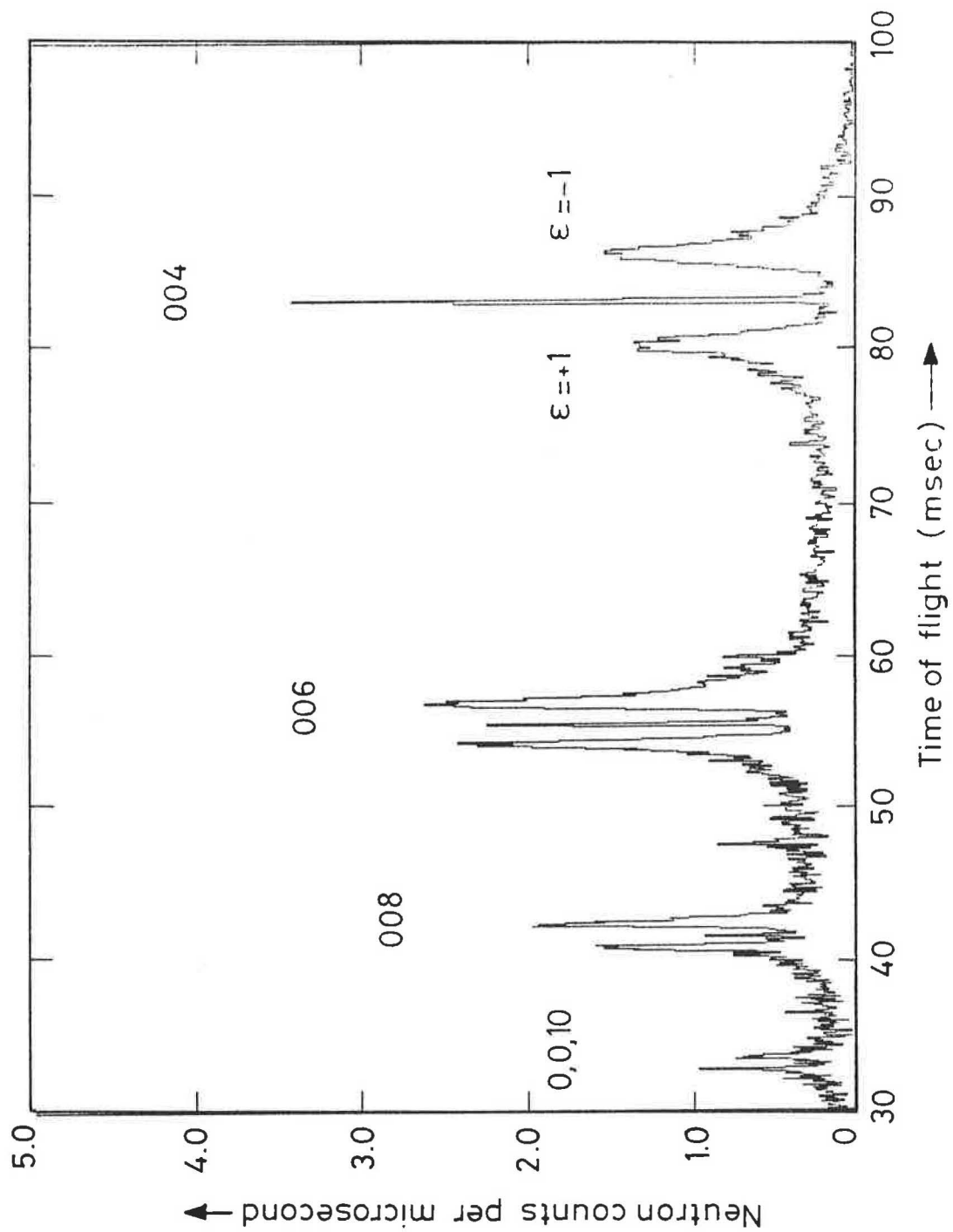


Figure 2: (b) One-phonon thermal diffuse scattering peaks recorded in a detector element offset from the Bragg scattering angle by $\Delta 2\theta = 2\theta - 2\theta_B = 3.2^\circ$.

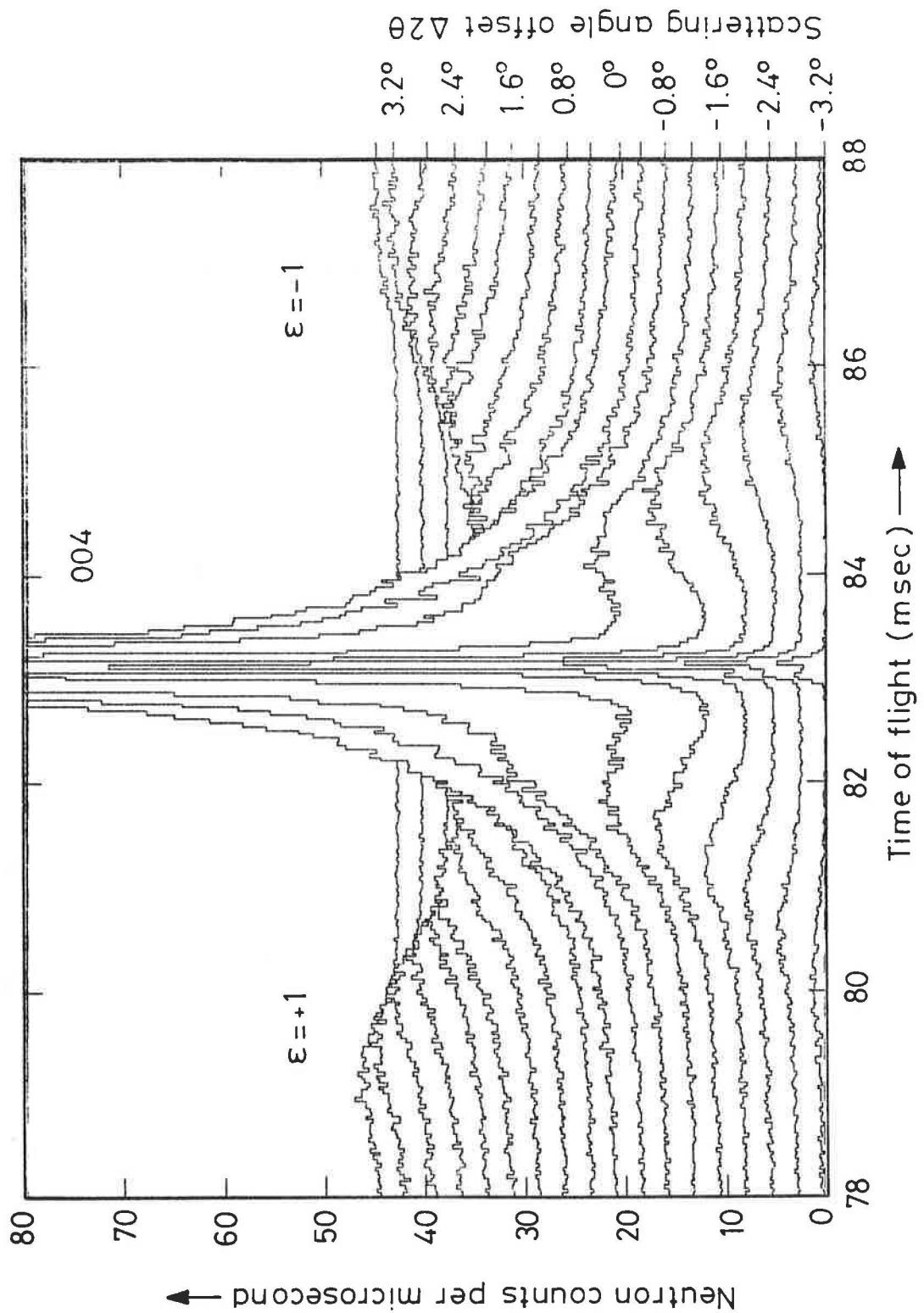


Figure 3: The scattering pattern around the (004) reflection from pyrolytic graphite showing the variation in the thermal diffuse scattering intensity as a function of time-of-flight and scattering angle offset $\Delta 2\theta$ from the Bragg angle.

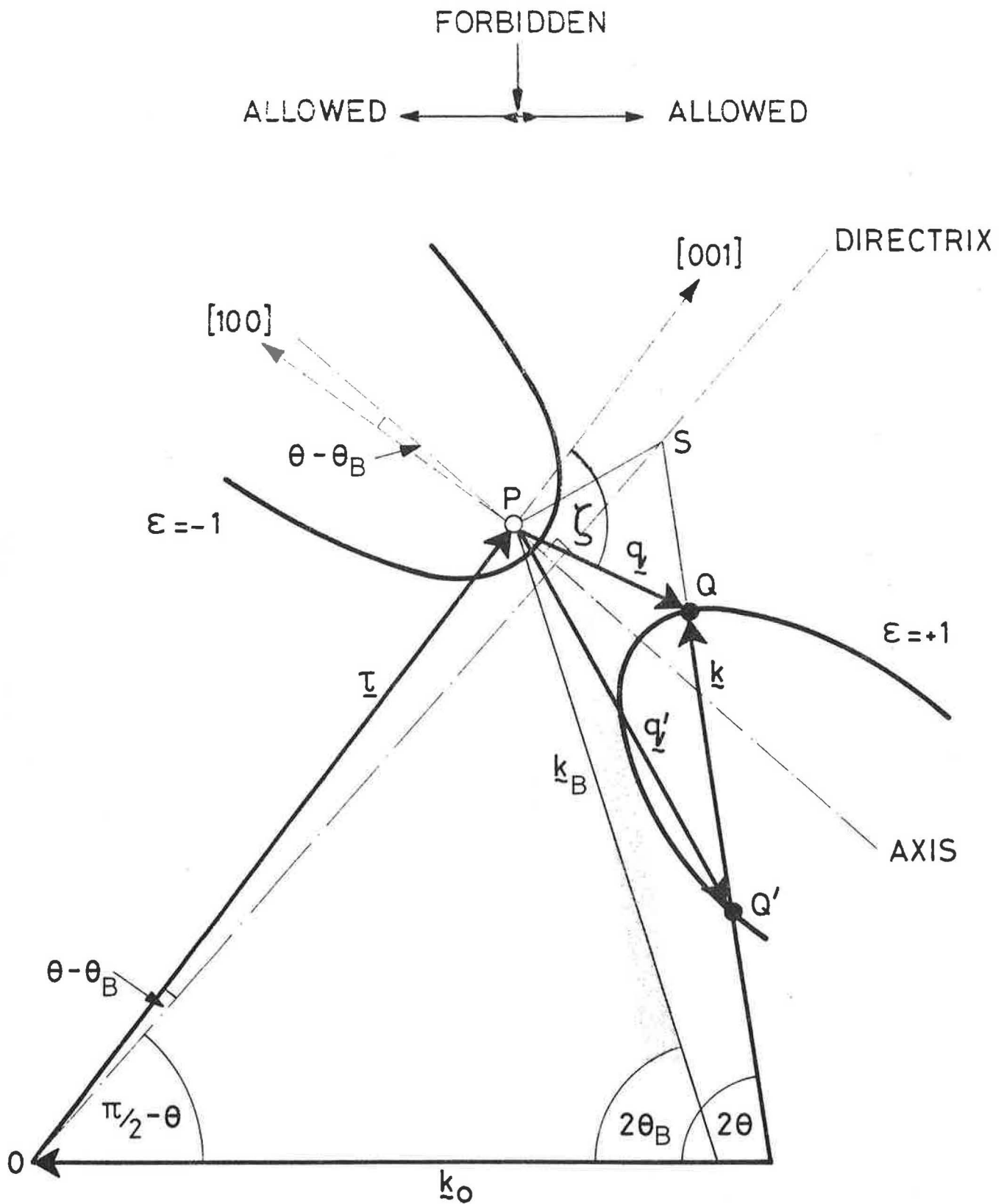


Figure 4: A representation of the scattering process in reciprocal space showing the hyperbolic scattering surfaces and, as a shaded area, the forbidden region in which no thermal diffuse scattering is observed. For clarity the scattering angle 2θ is drawn as $\sim 80^\circ$ rather than $\sim 174^\circ$, as in the backscattering geometry used. The point S is the termination of the scattered vector \underline{k} for the elastic scattering process ($k=k_0$).

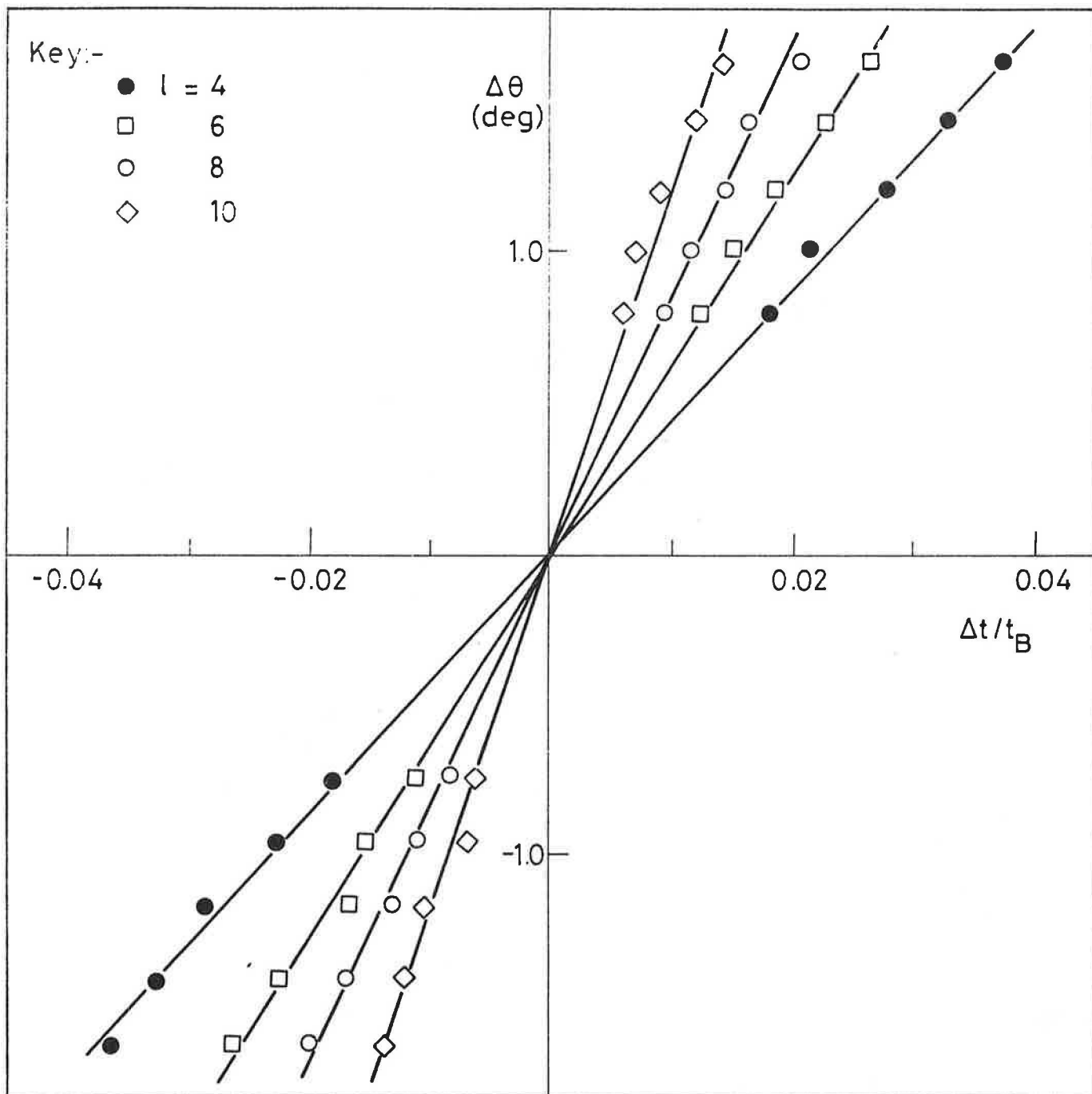


Figure 5: The displacements in time $\Delta t/t_B$ of the one-phonon thermal diffuse scattering peaks in graphite around the $00l$ reciprocal lattice points plotted as a function of the offset $\Delta\theta$ from the Bragg angle.

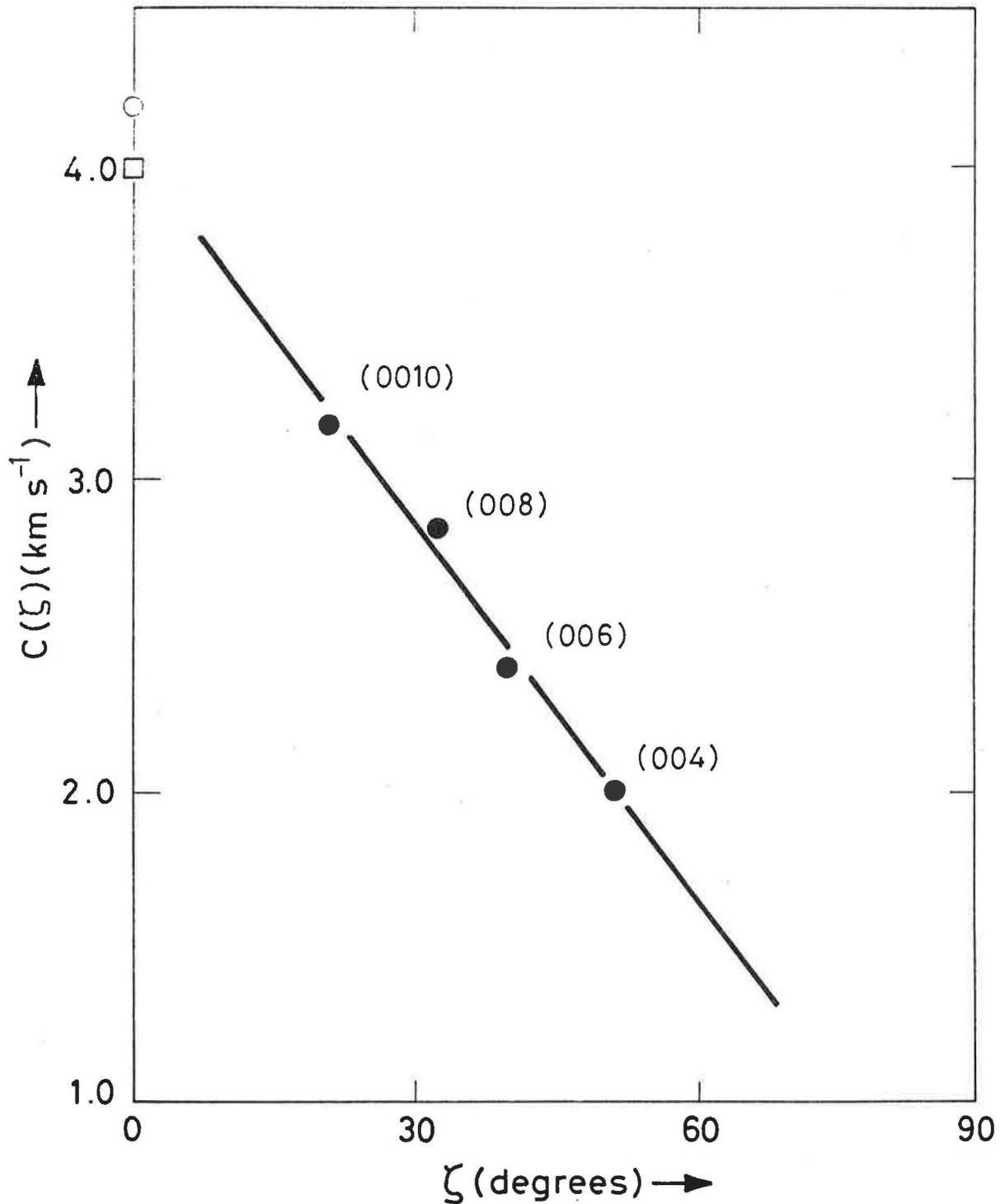


Figure 6: The phase velocity $c(\zeta)$ of the out-of-plane modes in pyrolytic graphite as a function of the angle between [001] and the propagation direction. The line is a least squares straight line fit to the data [●]. The symbol O indicates the velocity derived from phonon dispersion curve measurements by neutron scattering and □ the velocity determined by ultrasound measurements (Nicklow et al 1972).

